



# Extension of high-order harmonic generation cutoff from laser-ablated tin plasma plumes

WUFENG FU,<sup>1,2</sup> JUN WANG,<sup>3</sup>  JIAQI YU,<sup>1,2,4</sup>  AND WEI LI<sup>1,2,5</sup> 

<sup>1</sup>*GPL Photonics Laboratory, State Key Laboratory of Luminescence and Applications, Changchun Institute of Optics, Fine Mechanics and Physics, Chinese Academy of Sciences, Changchun, Jilin, 130033, China*

<sup>2</sup>*University of Chinese Academy of Sciences, Beijing 100049, China*

<sup>3</sup>*Institute of Atomic and Molecular Physics, Jilin University, Changchun 130012, China*

<sup>4</sup>*jiaqiyu@ciomp.ac.cn*

<sup>5</sup>*weili1@ciomp.ac.cn*

**Abstract:** The high-order harmonic spectra from laser-ablated tin plasma plumes are investigated experimentally and theoretically at different laser wavelengths. It is found that the harmonic cutoff is extended to ~84 eV and the harmonic yield is greatly improved by decreasing the driving laser wavelength from 800 nm to 400 nm. Applying the Perelomov-Popov-Terent'ev theory with the semiclassical cutoff law and one-dimensional time-dependent Schrödinger equation, the contribution of the Sn<sup>3+</sup> ion to harmonic generation accounts for the cutoff extension at 400 nm. With the qualitative analysis of the phase mismatching effect, we reveal the phase matching caused by the dispersion of free electrons is greatly optimized in the 400 nm driving field relative to the 800 nm driving field. The high-order harmonic generated from laser-ablated tin plasma plumes driven by the short laser wavelength provides a promising way to extend cutoff energy and generate intensely coherent extreme ultraviolet radiation.

© 2023 Optica Publishing Group under the terms of the [Optica Open Access Publishing Agreement](#)

## 1. Introduction

High-order harmonic generation (HHG) driven by strong laser fields enables visible to infrared laser coherent up-conversion into the extreme ultraviolet region with ultrashort-time characteristics [1–3]. This technology is being widely used in attosecond scientific applications [4,5]. Over the decades, atoms and molecules in gas [6–9] have been the most common medium for HHG. To broaden the studied atomic species, laser-ablated plasma plumes (LPPs) are used as an alternative medium [10,11]. With the advantage of the resonant characteristics of special electronic structures in metal ions [12–14], the high-order harmonic spectra generated by some metal ions in LPPs can appear obvious resonance enhancement [15–19]. However, the harmonic cutoff of the high-order harmonics driven by LPPs is low, which seriously restricts the practical application of HHG from LPPs. How to improve the harmonic cutoff of LPPs without reducing the harmonic yield has always been a topic of great concern.

The basic process of the high-order harmonics generated by the low-density LPPs can be regarded as a quantum nonlinearity originating from atoms and ions, which is similar to the three-step model of gaseous atoms [20,21]. In the three-step model, the maximum energy of the radiated photon follows the cutoff law  $h\nu_{\max} = I_p + 3.17U_p$ , where the ponderomotive energy  $U_p$  is proportional to the square of laser wavelength  $\lambda$  and the laser intensity  $I$ ,  $I_p$  is the ionization potential of the particles. In the gaseous HHG, the extension of the harmonic cutoff has been achieved with great success by increasing the available laser wavelength  $\lambda$  [1,22,23] and the effective laser intensity  $I$  [24–26]. For LPPs, many reports have also used laser wavelengths at 1.3–1.8  $\mu\text{m}$  instead of 0.8  $\mu\text{m}$  to generate high-order harmonics [27–33]. Some experiments successfully extended the harmonic cutoff in carbon LPPs [27,30], accompanied by efficient harmonic generation [30], whereas others failed in extension of harmonic cutoff [28,29,31–33]. This means that using a long-wavelength laser to extend harmonic cutoff is not easy for HHG

in LPPs. Since the plasma itself contains a lot of electrons, it is almost impossible to achieve phase matching by suppressing the ionization rate like gaseous HHG. Meanwhile, the scaling of single atom response  $\lambda^{-(5\sim 6)}$  [34] may result in a low harmonic conversion efficiency, which also makes the measurement of harmonic cutoff arduously. An alternative method of using higher ionization potential to extend harmonic cutoff has attracted extensive attentions [35–39]. In the HHG experiments of manganese [38], vanadium [39] and titanium [37] LPPs, the third ionization potential was used to successfully extend the cutoff. However, further improving the ionization potential and solving the severe phase mismatch caused by free electron dispersion will become a challenge. Moreover, the harmonic conversion efficiency of these materials is relatively low [40,41], which limits their practical application. It is urgent to study a more suitable and convenient method from LPPs to extend harmonic cutoff and increase the harmonic yield at the same time.

In this work, we experimentally and theoretically investigate the high-order harmonic spectra from the laser-ablated tin plasma plumes (Sn-LPPs) at different laser wavelengths. The experimental results show that the highest observable harmonic cutoff at 800 nm laser driving wavelength is  $\sim 51$  eV (33<sup>rd</sup>), while it can be extended to  $\sim 84$  eV (27<sup>th</sup>) at 400 nm with a great improvement of the harmonic yield at the same time. By using the Perelomov-Popov-Terent'ev model [42] with the semiclassical cutoff law and one-dimensional time-dependent Schrödinger equation, the contribution of the Sn<sup>3+</sup> ion to harmonic generation is responsible for the cutoff extension at 400 nm. In addition, we qualitatively analyze the improvement of phase matching caused by the dispersion of free electrons in the 400 nm driving field relative to the 800 nm driving field. And the dependence of harmonic cutoff in a 400 nm driving field on the intensity of driving pulses demonstrates the robustness of our theoretical calculation.

## 2. Experimental and numerical methods

### 2.1. Experimental design

The homebuilt HHG setup employed in the present work is shown in Fig. 1. Two laser beams are split from a commercial 1kHz, 0.8  $\mu\text{m}$  Ti: sapphire amplifier system (Spectra Physics: Sprifire Ace). One 210 ps, 0.5 mJ laser beam is split from the amplified laser beam before time compression as the heating pulse (HP), and the other is temporally compressed to derive a 35fs, 5.5 mJ laser beam as the driving pulse (DP). HP is focused on the Sn sample surface by a 200 mm lens to generate the plasma plumes. The second harmonic (centered at 400 nm) is generated by a 0.5-mm-thick  $\beta$ -Barium borate (BBO) crystal with a conversion efficiency of  $\sim 25\%$  and separated from the fundamental pulses by two dichroic mirrors (DM). The half-wave plate (HWP) rotates the second harmonic to horizontal polarization. After the plasma plumes ablated by HP with a time delay of  $\sim 50$  ns, the horizontally polarized 400 nm laser beam served as DP is focused into Sn-LPPs through a spherical lens with a focal length of 300 mm to generate high-order harmonics. After passing through a narrow slit, the harmonics are reflected by a concave mirror onto a 1200 grooves/mm flat field grating, and then the dispersed harmonics are detected by a microchannel plate with a phosphor screen and recorded by a CCD camera. The integration time of the CCD camera is fixed at 200 ms. The intensity of each harmonic spectrum in this paper is related to the photon flux. The pulse width of DP at the location where DP interacted with the plasma plumes is estimated to be  $\sim 50$  fs due to the propagation of the optical path through the air.

### 2.2. Simulation methods

The Perelomov-Popov-Terent'ev (PPT) theory [42] is applicable not only for noble gases [43], but also for metals [44–46]. In atomic units, the total rate of PPT ionization is

$$w_{PPT}(F, \omega) = \sum_{q \geq q_{\min}}^{\infty} w_q(F, \omega) \quad (1)$$

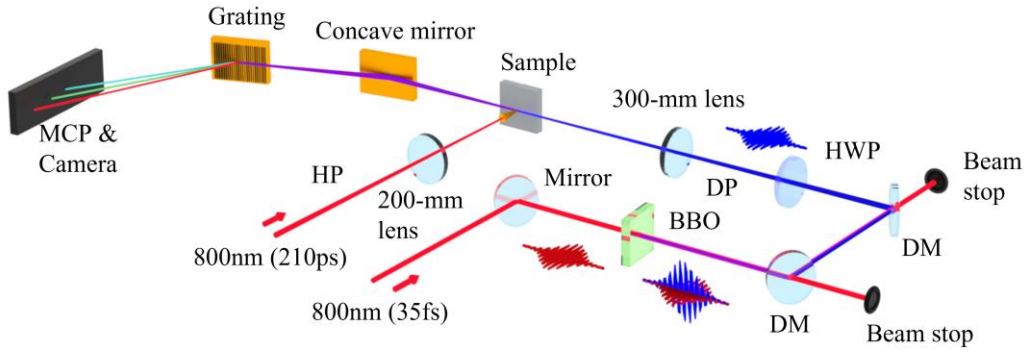


Fig. 1. Schematic diagram of the experimental setup.

where  $q_{\min}$  is equal to  $(I_p + U_p)/\omega$ , which represents the minimum number of photons required to reach the effective ionization potential  $I_p + U_p$ , and  $\omega$  and  $F$  are the frequency and amplitude of the laser field, respectively. The rate of PPT ionization can be also written as

$$w_{PPT}(F, \omega) = \frac{2^{2n^*}}{n^* \Gamma(n^* + l^* + 1) \Gamma(n^* - l^*)} \frac{(2l+1)(l+|m|)!}{2^{|m|} (|m|)! (l-|m|)!} I_p \left(\frac{2F_0}{F}\right)^{2n^* - |m| - 1} \times (1 + \gamma^2)^{|m|/2 + 3/4} A_m(\omega, \gamma) \exp\left[-\frac{2F_0}{3F} g(\gamma)\right] \quad (2)$$

with

$$g(\gamma) = \frac{3}{2\gamma} \left[ \left(1 + \frac{1}{2\gamma^2}\right) \sinh^{-1} \gamma - \frac{\sqrt{1 + \gamma^2}}{2\gamma} \right],$$

$$A_m(F, \omega) = \frac{4\gamma^2}{\sqrt{3\pi} |m|! (1 + \gamma^2)} \times \sum_{q \geq q_{\min}}^{\infty} e^{-\alpha(\gamma)(q-\nu)} \omega_m(\sqrt{\beta(\gamma)}(q - q_{\min})),$$

$$\omega_m(x) = \frac{x^{2|m|+1}}{2} \int_0^1 \frac{e^{-x^2 t} t^{|m|}}{\sqrt{1-t}} dt,$$

$$\alpha(\gamma) = 2 \left( \sinh^{-1} \gamma - \frac{\gamma}{\sqrt{1 + \gamma^2}} \right),$$

$$\beta(\gamma) = \frac{2\gamma}{\sqrt{1 + \gamma^2}},$$

where  $l$  and  $m$  are the orbital and magnetic quantum number of Sn ions,  $F_0 = (2I_p)^{3/2}$  is the Coulomb field,  $\gamma$  is the Keldysh parameter,  $\Gamma(x)$  is the gamma function,  $n^* = Z/\sqrt{2I_p}$  is the effective quantum number,  $l^* = n^* - 1$  is the effective orbital quantum number. Here,  $Z$  is the charge of Sn ions after absorbing  $q$  photons. The direction of laser polarization determines the quantization axis.

In the duration of the laser pulse, the ionization probability of Sn ions can be calculated from the PPT ionization rate by integration

$$P = 1 - \exp\left[-\int_{-\infty}^{+\infty} w(F_0(t)) dt\right] \quad (3)$$

where  $F_0(t)$  is a sine-squared envelope of the laser pulse, and the full width at half maximum (FWHM) of the envelope is the actual laser duration in our experiment. For each ionic species,

the ionization probability is calculated as a function of the laser intensity, as shown in Fig. 4(a) and Fig. 4(c).

We also calculate the high-order harmonic spectra from different Sn ions by one-dimensional time-dependent Schrödinger equation (1D-TDSE). In length gauge for this system, the corresponding 1D-TDSE, in atomic units, is given by

$$i \frac{\partial}{\partial t} \psi(x, t) = \left[ -\frac{1}{2} \frac{\partial^2}{\partial x^2} + V(x) + E(t) \cdot x \right] \psi(x, t) \quad (4)$$

By utilizing the split operator method [47], we are able to solve the 1D-TDSE in Eq. (4). To prevent the wave packet from being unphysical reflected off the boundary, a mask function of the kind  $\cos^{1/8}$  was employed. For the atomic potential function, a soft Coulomb function  $V(x) = -Z/\sqrt{x^2 + a}$  is utilized to prevent numerical inaccuracy brought on by the screening potential approaching the origin. Then, using Ehrenfest's theorem, the time-dependent induced dipole moment may be calculated as follows:

$$a(t) = \frac{\partial^2}{\partial t^2} \langle \psi(x, t) | x | \psi(x, t) \rangle = \left\langle \psi(x, t) \left| -\frac{dV(x)}{dx} - E(t) \right| \psi(x, t) \right\rangle \quad (5)$$

From the absolute square of the Fourier transformation of the time-dependent dipole accelerations, we may get the HHG power spectrum

$$P(\omega) = \left| \int e^{-i\omega t} a(t) dt \right|^2 \quad (6)$$

### 3. Results and discussion

The harmonic spectra driven by the 400 nm laser field at different HP intensities are measured first to optimize the harmonic generation condition, as shown in Fig. 2. Clearly, the harmonic cutoff at the HP intensity from  $0.8 \times 10^{10}$  W/cm<sup>2</sup> to  $1.4 \times 10^{10}$  W/cm<sup>2</sup> is about 17<sup>th</sup>, 23<sup>rd</sup>, 27<sup>th</sup> and 23<sup>rd</sup> order, respectively. This non-monotonic trend indicates that the harmonic cutoff value is influenced by the density of LPPs, which is related to the HP intensity. The cutoff value reaches a maximum of 27 at the HP intensity of  $1.2 \times 10^{10}$  W/cm<sup>2</sup>. As the HP intensity increases, the background noise caused by plasma line emissions becomes more prominent. The cutoff begins to get lower at the intensity of  $1.4 \times 10^{10}$  W/cm<sup>2</sup>. The harmonic spectra as a function of HP intensity are also measured in the driving field of 800 nm. It is found that the HP intensity of  $1.2 \times 10^{10}$  W/cm<sup>2</sup> is sufficient to give satisfactory harmonic spectrum in the driving fields of 400 nm and 800 nm without noticeable plasma emissions. Throughout the paper, we use a constant HP intensity at  $1.2 \times 10^{10}$  W/cm<sup>2</sup>. As shown in Fig. 2, we further observe a satellite peak on the right side of the 7<sup>th</sup> harmonic at 23.2 eV in the 400 nm driving field. This is most likely due to the second-order diffraction of the 15<sup>th</sup> harmonic [48,49]. And the 9<sup>th</sup> harmonic enhancement in all spectra is caused by the strong radiative transition of Sn<sup>2+</sup> ion from  $4d^{10}5s5p$  to  $4d^95s5p^2$ , which has been verified well in the theoretical calculation [50].

Figure 3 shows the harmonic spectra in the driving fields of 800 nm and 400 nm, respectively. In the 800 nm driving field, the 17<sup>th</sup> harmonic has a higher yield than the neighboring harmonics. This enhancement can be identified as the transition between two Sn<sup>+</sup> ionic states ( $4d^{10}5s^25p$  and  $4d^95s^25p^2$ ) with a frequency (26.22 eV) close to the 17<sup>th</sup> harmonic [51]. To achieve higher cutoff energy and have comparability at different laser wavelengths in the harmonic spectrum, the same camera integration time and gain factor are used in the measurement. Most notably, the harmonic cutoff in the 800 nm driving field is much higher than the previous reports [15,48], being about the 33<sup>rd</sup> order (~51 eV). And the cutoff in the 400 nm driving field can be further extended to around the 27<sup>th</sup> order (~84 eV). Interestingly, the cutoff energy is increased at short

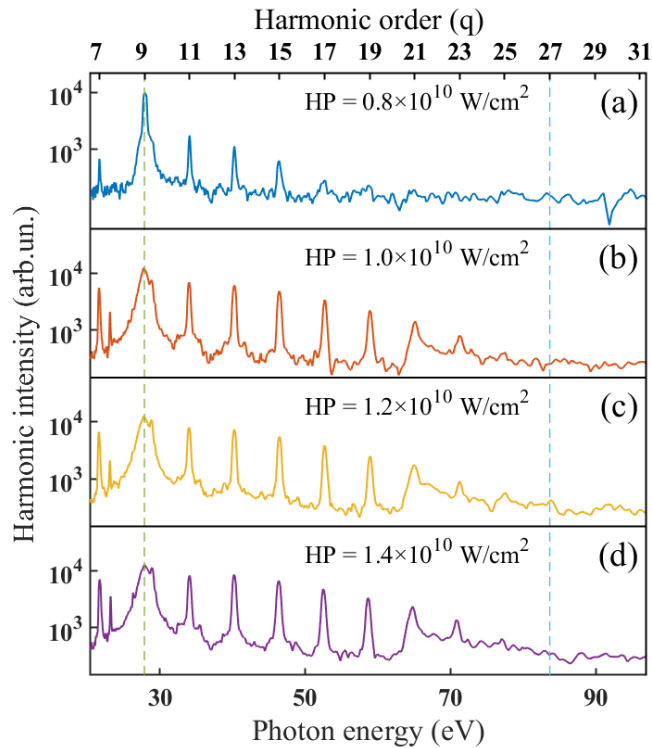


**Fig. 2.** High-order harmonic spectra generated from Sn-LPPs in the 400 nm driving field with HP intensity at (a)  $0.8 \times 10^{10}$  W/cm<sup>2</sup>, (b)  $1 \times 10^{10}$  W/cm<sup>2</sup>, (c)  $1.2 \times 10^{10}$  W/cm<sup>2</sup>, (d)  $1.4 \times 10^{10}$  W/cm<sup>2</sup>, respectively. The DP intensity is maintained at  $8 \times 10^{14}$  W/cm<sup>2</sup> for all the spectra.

wavelengths, in contrast to what is expected from the three-step model in gaseous HHG according to the semiclassical cutoff law. Moreover, the harmonic yield is also much improved at short wavelengths. We can observe that the harmonic yield of the 15<sup>th</sup> harmonic ( $\sim 46$  eV) in the driving field of 400 nm almost surpasses that of the 29<sup>th</sup> harmonic ( $\sim 45$  eV) in the driving field of 800 nm by 16 times. It is known that the conversion efficiency is the ratio of harmonic power to the laser power (photon energy  $\times$  photon flux/ laser power) [52]. In this experiment, the actual single pulse energies of 400 nm and 800 nm lasers are 350  $\mu$ J and 1600  $\mu$ J, respectively. Therefore, the actual harmonic conversion efficiency at 400 nm is 70 times higher than that at 800 nm, which is similar to the single-atom response ( $2^{5-6}$  times) [34].

To further investigate the inverse relationship between the harmonic cutoff and laser wavelength in Sn-LPPs HHG, the PPT model with the semiclassical cutoff law and 1D-TDSE methods are applied to distinguish the influenced factors in the microscopic particles, as shown in Fig. 4. Based on the physical picture of the three-step model, due to the depletion of the ground state (i.e. ionization probability reaches 99.9%), the harmonic cutoff energy cannot be further increased before the laser pulse reaches the peak intensity. The maximum value of the effective laser intensity is defined as the saturation intensity  $I_{\text{sat}}$ . To quantitatively describe the ionization process driven by 800 and 400 nm laser fields, the PPT theory is applied to estimate the  $I_{\text{sat}}$  of different Sn ions. Figure 4(a) shows the Sn ion yields as the function of DP intensity with 400 nm driving laser wavelength. The ionization probabilities of Sn<sup>+</sup>, Sn<sup>2+</sup> and Sn<sup>3+</sup> in a 400 nm driving field are saturated (i.e. 99.9%) at the intensities of  $0.09 \times 10^{14}$  W/cm<sup>2</sup>,  $4.07 \times 10^{14}$  W/cm<sup>2</sup> and  $8.33 \times 10^{14}$  W/cm<sup>2</sup>, respectively. According to the semiclassical cutoff law, the harmonic cutoff

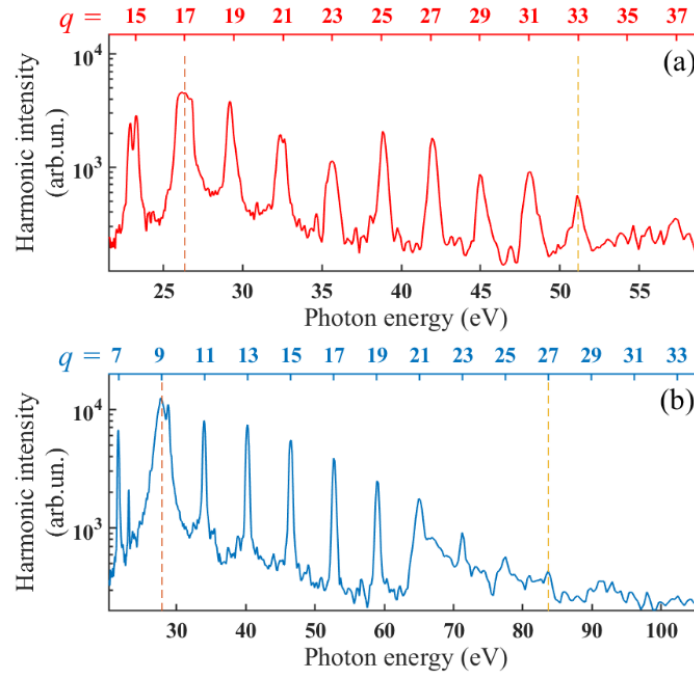


**Fig. 3.** High-order harmonic spectra generated from Sn-LPPs driven by (a) 800 nm laser field with DP intensity at  $9 \times 10^{14}$  W/cm<sup>2</sup>, and (b) 400 nm laser field with DP intensity at  $8 \times 10^{14}$  W/cm<sup>2</sup>. The HP intensity is maintained at  $1.2 \times 10^{10}$  W/cm<sup>2</sup> for all the spectra. The purpose of choosing DP with different intensities is to measure the maximum cutoff energy at different driving wavelengths.

of Sn<sup>3+</sup> at the saturation intensity is estimated to be the 25<sup>th</sup> harmonic, which is close to our experimental cutoff value. Therefore, the contribution of the Sn<sup>3+</sup> ion to harmonic generation is responsible for the extended harmonic cutoff of Sn-LPPs HHG driven by a 400 nm laser field. This assignment can be further confirmed by the method of 1D-TDSE as shown in Fig. 4(b). We summarize the cutoff energy obtained theoretically in Table 1. The results of the theoretical analysis are in good agreement with our experimental findings in a 400 nm laser field.

**Table 1. Calculated cutoff values in 400 and 800 nm driving fields from different ions using a semiclassical model and 1D-TDSE**

	400nm			800nm			
	$I_p$ (eV)	$I_{sat}$ (W/cm <sup>2</sup> )	$I_p+3.17U_p$ (eV)	1D-TDSE (eV)	$I_{sat}$ (W/cm <sup>2</sup> )	$I_p+3.17U_p$ (eV)	1D-TDSE (eV)
Sn <sup>+</sup>	14.63	$0.09 \times 10^{14}$	15.1 (5 <sup>th</sup> )	14.7 (5 <sup>th</sup> )	$0.48 \times 10^{14}$	23.33 (15 <sup>th</sup> )	23.2 (15 <sup>th</sup> )
Sn <sup>2+</sup>	30.51	$4.07 \times 10^{14}$	49.41 (16 <sup>th</sup> )	52.8 (17 <sup>th</sup> )	$5.66 \times 10^{14}$	124.48 (81 <sup>st</sup> )	136.7 (89 <sup>th</sup> )
Sn <sup>3+</sup>	40.74	$8.33 \times 10^{14}$	78.55 (25 <sup>th</sup> )	78.19 (25 <sup>th</sup> )	$10.33 \times 10^{14}$	229.79 (149 <sup>th</sup> )	229.79 (149 <sup>th</sup> )

Driven by 800 nm laser wavelength, the Sn<sup>3+</sup> ion yield exceeds 90% at the experimental laser intensity of  $9 \times 10^{14}$  W/cm<sup>2</sup> as shown in Fig. 4(c). It appears that the ionization of Sn<sup>3+</sup> may be contributed to the harmonic spectrum generated by the 800 nm laser field. However, the theoretically predicted cutoff from Sn<sup>3+</sup> at its saturation intensity is much higher than our experimental result and the previous measurements [15,48]. This is mainly due to the above theories without taking the macroscopical propagation effect into account. To achieve effective frequency up-conversion and optimize cutoff, the generated harmonic photons need to have the

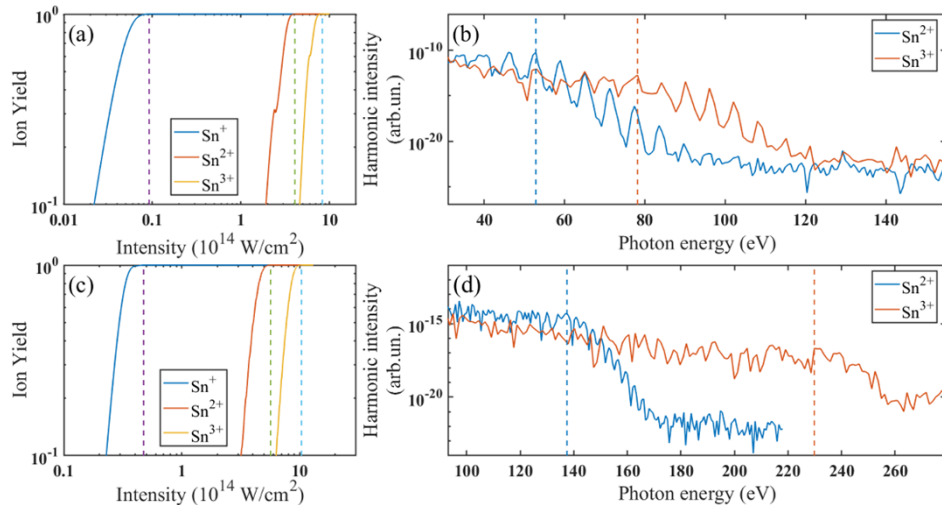


**Fig. 4.** Calculated ionization probabilities of different Sn ions as a function of DP intensity in (a) 400 nm, and (c) 800 nm laser fields. The saturation intensities  $I_{\text{sat}}$  of each particle is depicted by the vertical dash line. (b) and (d) show the calculated high-order harmonic spectra generated from  $\text{Sn}^{2+}$  and  $\text{Sn}^{3+}$  particles at each saturation intensity in 400 nm and 800 nm laser fields, respectively. The dashed lines represent the calculated harmonic cutoff, which is judged on the position of the sharp decrease in the harmonic intensity after a primary plateau.

same phase velocity as the driving field, i.e., the phase matching. The phase mismatching term  $\Delta k$  is a sum of contributions from the dispersion terms of atoms/ions, free electrons, quantum phase  $\Delta k_{\text{int}}$ , and laser geometry  $\Delta k_G$ . Although the focusing lens of DP is only 300 mm in our experiment, a few millimeters of Rayleigh length is still much longer than the plasma length of a hundred microns, which will cause the term  $\Delta k_G$  to be neglected [53–55]. For the term  $\Delta k_{\text{int}}$ , it is a function of  $\Delta I/\Delta z$ , and within the Rayleigh length, the change in DP intensity  $\Delta I$  near the plasma length  $\Delta z$  is very small [53,54]. Therefore, in comparison with the dispersion terms of atoms/ions and electrons, for Sn-LPPs HHG, the contributions of  $\Delta k_G$  and  $\Delta k_{\text{int}}$  to the phase mismatching are negligible [17,55]. To analyze the phase mismatching of Sn-LPPs HHG at different laser wavelengths, the term  $\Delta k$  can be simplified as

$$\Delta k = qk_\omega - k_{q\omega} \approx - \underbrace{\frac{n_i \omega_q}{c} (\delta + \Delta\delta)}_{\text{atom and ions}} + \underbrace{\frac{\omega_q n_e e^2}{c \epsilon_0 m \omega_{DP}^2}}_{\text{free electrons}} \quad (7)$$

where  $\omega_q$  is the  $q^{\text{th}}$  harmonic frequency,  $\omega_{DP}$  is the DP frequency,  $\epsilon_0$  is the vacuum permittivity,  $m$  is the electron mass,  $\delta$  is the refractive index difference between DP and the harmonic from different ions,  $\Delta\delta$  is the nonlinear refractive index from different ions,  $n_i$  is the density of different particles of Sn and  $i=0$  denotes atoms,  $i=1, 2, 3, \dots$  denote ions with different charges, respectively. In a multi-species plasma medium, the free electron term plays a major role in the phase mismatching [17,55], whereas the atomic term is replaced by the linear dispersion and the Kerr effect of the ion to compensate for the electronic dispersion term and achieve phase matching. It has been demonstrated that the dispersion of ions is negative and increases with laser frequency  $\omega_{DP}$  [55]. The free electron term is positive and inversely proportional to the square of laser frequency  $\omega_{DP}$ , therefore, the perfect agreement between theory and experiment

in the 400 nm driving field is due to the improvement of phase matching in the 400 nm driving field compared with the 800 nm driving field.

Figure 5 shows the harmonic cutoff as a function of DP intensity in the 400 nm driving field. There is a small plateau at the 15<sup>th</sup> order, and the cutoff value remains constant after reaching the 27<sup>th</sup> order. According to the PPT theory, the ionization process has a window where the  $\text{Sn}^{2+}$  yield is saturated and the  $\text{Sn}^{3+}$  ions cannot achieve effective ionization within the intensity ranges from  $3.99 \times 10^{14} \text{ W/cm}^2$  to  $4.62 \times 10^{14} \text{ W/cm}^2$ . The cutoff will be the same in this intensity region, thus, the first cutoff plateau is derived from the contribution of the  $\text{Sn}^{2+}$  ion to harmonic generation. In the same way, the second cutoff plateau at the 27<sup>th</sup> order corresponds to the contribution of the  $\text{Sn}^{3+}$  ion to harmonic generation. However, the ionization of the  $\text{Sn}^{4+}$  ion needs the peak laser intensity to reach  $3 \times 10^{15} \text{ W/cm}^2$ , which is a harsh experimental condition. Therefore, the cutoff value remains constant at the intensity ranges from  $8 \times 10^{14} \text{ W/cm}^2$  to  $1.4 \times 10^{15} \text{ W/cm}^2$ .

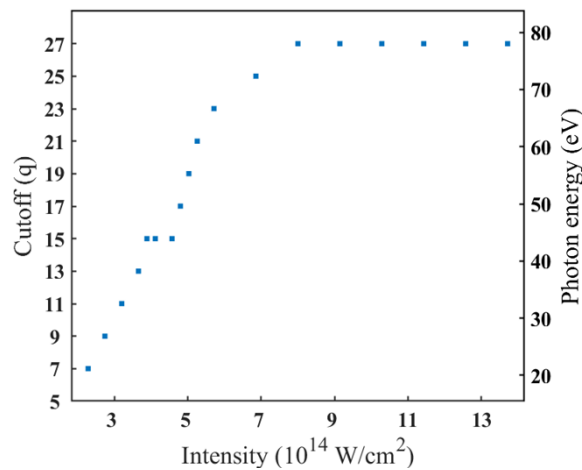


**Fig. 5.** Dependence of the harmonic cutoff in the 400 nm driving field on DP intensity.

#### 4. Conclusion

In summary, we have studied the high-order harmonic spectra of Sn-LPPs in 800 and 400 nm driving fields. Experimental measurement shows a simultaneous enhancement of the harmonic cutoff and the harmonic yield at the short laser wavelength. This enhancement in synchronization has not been achieved in previous HHG experiments of LPPs. Theoretical calculations are in good agreement with our result in the 400 nm driving field, which confirms that the contribution of the  $\text{Sn}^{3+}$  ion to harmonic generation accounts for the cutoff extension at 400 nm. Considering the propagation effect in experimental measurements, we reveal the phase matching caused by the dispersion of free electrons is much improved in the 400 nm driving field relative to the 800 nm driving field. Two cutoff plateaus in dependence with DP intensity at 400 nm laser wavelength can also be well described by our theories even without consideration of the phase matching effect, clarifying the robustness of our theoretical calculation. We prove that the high-order harmonic generated from laser-ablated tin plasma plumes driven by a short laser wavelength effectively extends the cutoff energy and generates intensely coherent extreme ultraviolet radiation.

**Funding.** National Natural Science Foundation of China (62121005, 62134009); Changchun Institute of Optics, Fine Mechanics and Physics, Chinese Academy of Sciences; Department of Science and Technology of Jilin Province (YDZJ202102CXJD002).

**Acknowledgments.** We thank Dianxiang Ren and Yu Hang Lai for interesting discussions.

**Disclosures.** The authors declare no competing financial interest.

**Data availability.** Data underlying the results presented in this paper are not publicly available at this time but may be obtained from the authors upon reasonable request.

## References

1. T. Popmintchev, M.-C. Chen, and D. Popmintchev, *et al.*, “Bright coherent ultrahigh harmonics in the keV X-ray regime from mid-infrared femtosecond lasers,” *Science* **336**(6086), 1287–1291 (2012).
2. J. Li, X. Ren, Y. Yin, K. Zhao, A. Chew, Y. Cheng, E. Cunningham, Y. Wang, S. Hu, Y. Wu, M. Chini, and Z. Chang, “53-attosecond X-ray pulses reach the carbon K-edge,” *Nat. Commun.* **8**(1), 186–190 (2017).
3. T. Gaumnitz, A. Jain, Y. Pertot, M. Huppert, I. Jordan, F. Ardana-Lamas, and H. J. Wörner, “Streaking of 43-attosecond soft-X-ray pulses generated by a passively CEP-stable mid-infrared driver,” *Opt. Express* **25**(22), 27506–27518 (2017).
4. F. Schlaepfer, M. Lucchini, S. A. Sato, M. Volkov, L. Kasmi, N. Hartmann, A. Rubio, L. Gallmann, and U. Keller, “Attosecond optical-field-enhanced carrier injection into the GaAs conduction band,” *Nat. Phys.* **14**(6), 560–564 (2018).
5. L. He, S. Sun, P. Lan, Y. He, B. Wang, P. Wang, X. Zhu, L. Li, W. Cao, P. Lu, and C. D. Lin, “Filming movies of attosecond charge migration in single molecules with high harmonic spectroscopy,” *Nat. Commun.* **13**(1), 4595–4603 (2022).
6. M. Ferray, A. L. Huillier, X. F. Li, L. A. Lompre, G. Mainfray, and C. Manus, “Multiple-harmonic conversion of 1064 nm radiation in rare gases,” *J. Phys. B: At., Mol. Opt. Phys.* **21**(3), L31–L35 (1988).
7. N. Kanda, T. Imahoko, K. Yoshida, A. Tanabashi, A. Amani Eilanlou, Y. Nabekawa, T. Sumiyoshi, M. Kuwata-Gonokami, and K. Midorikawa, “Opening a new route to multiphoton coherent XUV sources via intracavity high-order harmonic generation,” *Light: Sci. Appl.* **9**(1), 168–176 (2020).
8. Y. Pan, S.-F. Zhao, and X.-X. Zhou, “Generation of isolated sub-40-as pulses from gas-phase CO molecules using an intense few-cycle chirped laser and a unipolar pulse,” *Phys. Rev. A* **87**(3), 035805 (2013).
9. Q. Gao, S. Chen, H. Liang, Y. Wang, C. Bi, S. Ben, R. Ma, D. Ding, and J. Chen, “Comparison study on atomic and molecular ellipticity dependence of high-order harmonic generation,” *Phys. Rev. A* **103**(4), 043115 (2021).
10. W. Fu, Y. H. Lai, J. Liang, and W. Li, “Investigation of high-harmonic cutoff of metal ions driven by near-infrared laser,” *Opt. Express* **30**(13), 23090–23101 (2022).
11. W. Fu, Y. H. Lai, and W. Li, “Comparative study of medium length-dependent high-harmonic generation from metal ions,” *Opt. Express* **30**(26), 47315–47325 (2022).
12. V. Strelkov, “Role of autoionizing state in resonant high-order harmonic generation and attosecond pulse production,” *Phys. Rev. Lett.* **104**(12), 123901 (2010).
13. M. A. Fareed, V. V. Strelkov, N. Thiré, S. Mondal, B. E. Schmidt, F. Légaré, and T. Ozaki, “High-order harmonic generation from the dressed autoionizing states,” *Nat. Commun.* **8**(1), 16061–16065 (2017).
14. M. A. Khokhlova, M. Y. Emelin, M. Y. Ryabikin, and V. V. Strelkov, “Polarization control of quasimonochromatic XUV light produced via resonant high-order harmonic generation,” *Phys. Rev. A* **103**(4), 043114 (2021).
15. M. Suzuki, M. Baba, R. Ganeev, H. Kuroda, and T. Ozaki, “Anomalous enhancement of a single high-order harmonic by using a laser-ablation tin plume at 47 nm,” *Opt. Lett.* **31**(22), 3306–3308 (2006).
16. R. A. Ganeev, M. Suzuki, M. Baba, H. Kuroda, and T. Ozaki, “Strong resonance enhancement of a single harmonic generated in the extreme ultraviolet range,” *Opt. Lett.* **31**(11), 1699–1701 (2006).
17. N. Rosenthal and G. Marcus, “Discriminating between the role of phase matching and that of the single-atom response in resonance plasma-plume high-order harmonic generation,” *Phys. Rev. Lett.* **115**(13), 133901 (2015).
18. M. Singh, M. A. Fareed, V. Strelkov, A. N. Grum-Grzhimailo, A. Magunov, A. Laramée, F. Légaré, and T. Ozaki, “Intense quasi-monochromatic resonant harmonic generation in the multiphoton ionization regime,” *Optica* **8**(8), 1122–1125 (2021).
19. J. Liang, Y. H. Lai, W. Fu, C. Guo, and W. Li, “Distinguishing monomer and nanoparticle contributions to high-harmonic emission from laser-ablated plumes,” *Opt. Express* **29**(15), 23421–23429 (2021).
20. P. B. Corkum, “Plasma perspective on strong field multiphoton ionization,” *Phys. Rev. Lett.* **71**(13), 1994–1997 (1993).
21. M. Lewenstein, P. Balcou, M. Y. Ivanov, A. L’Huillier, and P. B. Corkum, “Theory of high-harmonic generation by low-frequency laser fields,” *Phys. Rev. A* **49**(3), 2117–2132 (1994).
22. B. Shan and Z. Chang, “Dramatic extension of the high-order harmonic cutoff by using a long-wavelength driving field,” *Phys. Rev. A* **65**(1), 011804 (2001).
23. E. J. Takahashi, T. Kanai, K. L. Ishikawa, Y. Nabekawa, and K. Midorikawa, “Coherent Water Window X Ray by Phase-Matched High-Order Harmonic Generation in Neutral Media,” *Phys. Rev. Lett.* **101**(25), 253901 (2008).
24. J. Seres, E. Seres, A. J. Verhoef, G. Tempea, C. Strelci, P. Wobrauschek, V. Yakovlev, A. Scrinzi, C. Spielmann, and F. Krausz, “Source of coherent kiloelectronvolt X-rays,” *Nature* **433**(7026), 596 (2005).
25. D. M. Gaudiosi, B. Reagan, T. Popmintchev, M. Grisham, M. Berrill, O. Cohen, B. C. Walker, M. M. Murnane, H. C. Kapteyn, and J. J. Rocca, “High-order harmonic generation from ions in a capillary discharge,” *Phys. Rev. Lett.* **96**(20), 203001 (2006).
26. D. Popmintchev, C. Hernández-García, and F. Dollar, *et al.*, “Ultraviolet surprise: Efficient soft X-ray high-harmonic generation in multiply ionized plasmas,” *Science* **350**(6265), 1225–1231 (2015).

27. R. A. Ganeev, C. Hutchison, T. Witting, F. Frank, W. A. Okell, A. Zaïr, S. Weber, P. V. Redkin, D. Y. Lei, T. Roschuk, S. A. Maier, I. López-Quintás, M. Martín, M. Castillejo, J. W. G. Tisch, and J. P. Marangos, "High-order harmonic generation in graphite plasma plumes using ultrashort laser pulses: a systematic analysis of harmonic radiation and plasma conditions," *J. Phys. B: At., Mol. Opt. Phys.* **45**(16), 165402 (2012).
28. R. A. Ganeev, C. Hutchison, T. Witting, F. Frank, S. Weber, W. A. Okell, E. Fiordilino, D. Cricchio, F. Persico, A. Zaïr, J. W. G. Tisch, and J. P. Marangos, "High-order harmonic generation in fullerenes using few- and multi-cycle pulses of different wavelengths," *J. Opt. Soc. Am. B* **30**(1), 7–12 (2013).
29. A. S. Emelina, M. Y. Emelin, R. A. Ganeev, M. Suzuki, H. Kuroda, and V. V. Strelkov, "Two-color high-harmonic generation in plasmas: efficiency dependence on the generating particle properties," *Opt. Express* **24**(13), 13971–13983 (2016).
30. M. A. Fareed, N. Thiré, S. Mondal, B. E. Schmidt, F. Légaré, and T. Ozaki, "Efficient generation of sub-100 eV high-order harmonics from carbon molecules using infrared laser pulses," *Appl. Phys. Lett.* **108**(12), 124104–124107 (2016).
31. R. A. Ganeev, Z. Wang, P. Lan, P. Lu, M. Suzuki, and H. Kuroda, "Indium plasma in single- and two-color mid-infrared fields: Enhancement of tunable harmonics," *Phys. Rev. A* **93**(4), 043848 (2016).
32. R. A. Ganeev, "Enhancement of high-order harmonics generated in laser-produced plasma using ionic resonances and nanoparticles," *Opt. Spectrosc.* **122**(2), 250–268 (2017).
33. R. A. Ganeev and H. Kuroda, "High-order harmonics generation in atomic and molecular zinc plasmas," *Photonics* **8**(2), 29–40 (2021).
34. E. L. Falcão-Filho, V. M. Gkortsas, A. Gordon, and F. X. Kärtner, "Analytic scaling analysis of high harmonic generation conversion efficiency," *Opt. Express* **17**(13), 11217–11229 (2009).
35. R. Ganeev, M. Suzuki, M. Baba, H. Kuroda, and T. Ozaki, "High-order harmonic generation from boron plasma in the extreme-ultraviolet range," *Opt. Lett.* **30**(7), 768–770 (2005).
36. R. A. Ganeev, M. Baba, M. Suzuki, and H. Kuroda, "High-order harmonic generation from silver plasma," *Phys. Lett. A* **339**(1-2), 103–109 (2005).
37. M. Suzuki, R. A. Ganeev, L. B. E. Bom, M. Baba, T. Ozaki, and H. Kuroda, "Extension of cutoff in high harmonic by using doubly charged ions in a laser-ablation plume," *J. Opt. Soc. Am. B* **24**(11), 2847–2852 (2007).
38. R. A. Ganeev, L. B. E. Bom, J. C. Kieffer, M. Suzuki, H. Kuroda, and T. Ozaki, "Demonstration of the 101st harmonic generated from a laser-produced manganese plasma," *Phys. Rev. A* **76**(2), 023831 (2007).
39. M. Suzuki, L. B. E. Bom, T. Ozaki, R. A. Ganeev, M. Baba, and H. Kuroda, "Seventy-first harmonic generation from doubly charged ions in preformed laser-ablation vanadium plume at 110 eV," *Opt. Express* **15**(7), 4112–4117 (2007).
40. G. S. Boltaev, V. V. Kim, M. Iqbal, N. A. Abbasi, V. S. Yalishiev, R. A. Ganeev, and A. S. Alnaser, "Application of 150 kHz Laser for High-Order Harmonic Generation in Different Plasmas," *Photonics* **7**(3), 66–78 (2020).
41. M. Suzuki, M. Baba, R. Ganeev, H. Kuroda, and T. Ozaki, "High-Order Harmonic Generation From Laser-Ablated Plasma Plume Pumped by Femtosecond Laser Pulse," in *X-Ray Lasers 2006: Proceedings of the 10th International Conference*, (Springer, 2007), 395–400.
42. A. M. Perelomov, V. S. Popov, and M. V. Terent'ev, "Ionization of atoms in an alternating electric field," *Sov. Phys. JETP* **23**(5), 924–934 (1966).
43. S.-F. Zhao, A.-T. Le, C. Jin, X. Wang, and C. D. Lin, "Analytical model for calibrating laser intensity in strong-field-ionization experiments," *Phys. Rev. A* **93**(2), 023413 (2016).
44. Y. H. Lai, J. Xu, U. B. Szafruga, B. K. Talbert, X. Gong, K. Zhang, H. Fuest, M. F. Kling, C. I. Blaga, P. Agostini, and L. F. DiMauro, "Experimental investigation of strong-field-ionization theories for laser fields from visible to midinfrared frequencies," *Phys. Rev. A* **96**(6), 063417 (2017).
45. H. Kang, S. Chen, Z. Lin, W. Chu, J. Yao, W. Quan, J. Chen, X. Liu, Y. Cheng, and Z. Xu, "Comparative study of strong-field ionization of alkaline-earth-metal atoms," *Phys. Rev. A* **101**(5), 053433 (2020).
46. Y. H. Lai, X. Wang, Y. Li, X. Gong, B. K. Talbert, C. I. Blaga, P. Agostini, and L. F. DiMauro, "Experimental test of recollision effects in double ionization of magnesium by near-infrared circularly polarized fields," *Phys. Rev. A* **101**(1), 013405 (2020).
47. M. R. Hermann and J. Fleck Jr., "Split-operator spectral method for solving the time-dependent Schrödinger equation in spherical coordinates," *Phys. Rev. A* **38**(12), 6000–6012 (1988).
48. R. A. Ganeev, H. Singhal, P. A. Naik, U. Chakravarty, V. Arora, J. A. Chakera, R. A. Khan, M. Raghuramaiah, S. R. Kumbhare, R. P. Kushwaha, and P. D. Gupta, "Optimization of the high-order harmonics generated from silver plasma," *Appl. Phys. B* **87**(2), 243–247 (2007).
49. R. A. Ganeev, H. Singhal, P. A. Naik, I. A. Kulagin, P. V. Redkin, J. A. Chakera, M. Tayyab, R. A. Khan, and P. D. Gupta, "Enhancement of high-order harmonic generation using a two-color pump in plasma plumes," *Phys. Rev. A* **80**(3), 033845 (2009).
50. R. A. Ganeev, V. V. Strelkov, C. Hutchison, A. Zaïr, D. Kilbane, M. A. Khokhlova, and J. P. Marangos, "Experimental and theoretical studies of two-color-pump resonance-induced enhancement of odd and even harmonics from a tin plasma," *Phys. Rev. A* **85**(2), 023832 (2012).
51. D. Grainne, K. Paul van, and D. Padraig, "4d→5p transitions in the extreme ultraviolet photoabsorption spectra of Sn II and Sn III," *J. Phys. B: At., Mol. Opt. Phys.* **34**(15), 3171–3178 (2001).
52. H. Wang, Y. Xu, S. Ulonska, J. S. Robinson, P. Ranitovic, and R. A. Kaindl, "Bright high-repetition-rate source of narrowband extreme-ultraviolet harmonics beyond 22 eV," *Nat. Commun.* **6**(1), 7459–7465 (2015).

53. S. Kazamias, D. Douillet, F. Weihe, C. Valentin, A. Rousse, S. Sebban, G. Grillon, F. Auge, D. Hulin, and P. Balcou, "Global optimization of high harmonic generation," *Phys. Rev. Lett.* **90**(19), 193901 (2003).
54. H.-W. Sun, P.-C. Huang, Y.-H. Tzeng, J.-T. Huang, C. D. Lin, C. Jin, and M.-C. Chen, "Extended phase matching of high harmonic generation by plasma-induced defocusing," *Optica* **4**(8), 976–981 (2017).
55. H. Singhal, V. Arora, B. S. Rao, P. A. Naik, U. Chakravarty, R. A. Khan, and P. D. Gupta, "Dependence of high-order harmonic intensity on the length of preformed plasma plumes," *Phys. Rev. A* **79**(2), 023807 (2009).